Laboratory Simulations of Controlled Energetic Electron-Beam-Plasma Interactions in Space

E. P. Szuszczewicz*
E. O. Hulburt Center for Space Research, Naval Research Laboratory, Washington, D.C.

Recent laboratory investigations of space-simulated electron-beam-plasma interactions have concentrated on the transition from single-particle behavior to collective plasma processes with emphasis on the beam-plasma discharge. The plasma has been characterized with respect to its spatial distributions in density, temperature, and density fluctuation power spectra. The latter results have been further classified in terms of amplitude and spectral distributions. The overall results include 1) detailed radial profiles of plasma density as a function of beam parameters; 2) association of low-frequency large-amplitude fluctuations with ion acoustic, ion cyclotron, and drift-wave modes; 3) identification and spatial mapping of suprathermal electrons in the beam core; and 4) experimental definition of a density-dependent criterion for the ignition of the beam-plasma discharge. The data provide a synoptic perspective on accumulated rocket observations and meaningfully contribute to planning activities for future space-borne applications of artificially injected energetic electron beams.

Nomenclature

B = magnetic field
c = velocity of light
E = electron energy
f = frequency
$I_B, \delta I_B$ = baseline probe current and associated fluctuations at fixed potential V_B
I_c = critical beam current for beam-plasma discharge ignition
I_e^{sat} = electron saturation current
k = wavelength $2\pi/\lambda$ or Boltzmann constant when used with T_e
L = beam-plasma system length
m_e, m_i = electron and ion mass
$N_e, \delta N_e$ = electron density and associated fluctuations
N_i = ion density
P = neutral gas pressure
R_p = probe (or Shuttle) radius
R_s = sheath radius
S = dimensionless sheath size
T_e = electron temperature
V_a = Alfvén velocity $= B/(4\pi N_i m_i)^{1/2}$
V_b = energetic electron beam accelerating potential
V_B = fixed baseline probe potential
V_∞ = plasma potential
v_s = ion sound speed $= (kT_e/m_i)^{1/2}$
β = thermal/magnetic energy ratio $= 8\pi N_e kT_e/B^2$
θ = angle relative to magnetic field
λ = wavelength
λ_D = Debye length $= (kT_e/4\pi N_e e^2)^{1/2}$
ϕ_p = probe (or Shuttle) potential
$\omega_c^{e(i)}/2\pi$ = electron (ion) cyclotron frequency $= eB/2\pi m_{e(i)} c$
$\omega_D/2\pi$ = electron drift frequency $= kT_e(dN_e/dx)/eB\lambda N_e$
$\omega_p^{e(i)}/2\pi$ = electron (ion) plasma frequency $= (N_e e^2/\pi m_{e(i)})^{1/2}$
$\omega_u/2\pi$ = upper hybrid frequency $= [(\omega_p^e)^2 + (\omega_c^e)^2]^{1/2}/2\pi$

Presented as part of Paper 82-0146 at the AIAA 20th Aerospace Sciences Meeting, Orlando, Fla., Jan. 11-14, 1982; submitted Jan. 22, 1982; revision received Sept. 7, 1982.

*Head, Ionospheric Diagnostics Section, Space Science Division.

Introduction

FROM the time of the early experiments involving plasma oscillations,[1-4] there has been continued interest in the collective interactions of charged-particle beams and plasmas. This interest has evolved from studies of various small-scale laboratory gas discharges into research on controlled thermonuclear reactions, and recently into the application of charged-particle beams in space. These efforts have made it strikingly clear that rarely is a beam-plasma system quiescent. In fact, it is characteristic of beam-plasma systems to manifest a number of instability mechanisms with attendant and varied levels of plasma turbulence.

Within the space science community, interest in artificially injected electron beams came about largely from a perspective that viewed the beams as diagnostic devices to probe various aspects of ionospheric and magnetospheric phenomena.[5-14] The applications included the mapping of geomagnetic field lines; detection of geomagnetic conjugates by the generation of artificial aurora; the study of beam spreading, atmospheric excitation, and ionization processes; and the measurement of magnetic field aligned potentials. (See Ref. 14 for an excellent bibliography and chronology of rocket-borne beam experiments and their associated results.) On the other hand, interest in nonlinear beam-plasma processes arose in a less direct fashion. The early rocket experiments resulted in a number of puzzles, not only in unexplained beam particle behavior and vehicle neutralization processes, but also in the characteristics of emitted plasma waves. In some cases the results were at such variance with expectations that a beam-plasma instability process was suspected of playing a dominant role. A series of laboratory simulations[15-17] then accumulated substantial information which now seems to have definitively identified the fundamental process as the beam-plasma discharge (BPD).[18,19]

The BPD is the result of a two-stream beam-plasma instability that appears at a critical beam current I_c given approximately by

$$I_c\,[\text{amps}] = 6\times 10^{-11} V_b^{3/2}/PLB^{0.7} \qquad (1)$$

where the beam energy V_b is in volts, the superimposed magnetic field B in gauss, the pressure P in torr, and system length L (gun-to-collector distance) in meters. [Equation (1) is an empirical fit to the original laboratory studies[17] for parallel injection and represents that data to an accuracy better than 40%.] This critical current level yields an in-

creased ion-pair production rate, enhanced 3914 Å emission, a modification of the primary beam velocity, and emission of high-frequency waves.

In the pre-BPD case ($I<I_c$), the beam energy distribution is sharply peaked at the acceleration potential,[20,21] and the high-frequency wave emissions are usually localized to narrow bands slightly greater than the electron cyclotron frequency $\omega_c^e/2\pi$, with higher harmonics of decreasing amplitude.[17] The amplitude and frequency of the narrow-band emission is observed to increase with beam current.[16] Assuming that density varied with beam current, the latter result suggested that the waves were at the upper hybrid frequency $\omega_u/2\pi$ rather than at $\omega_c^e/2\pi$. In addition to the narrow-band emissions there are low-frequency waves concentrated at the low end of the spectrum, rising steeply below the ion plasma frequency $\omega_p^i/2\pi$ ($\sim$100 kHz).

When the BPD is ignited ($I\geq I_c$), the entire band up to the electron cyclotron frequency is occupied by intense emissions of featureless spectral characteristics. In addition, an intense higher-frequency band of emissions appears at or near the local plasma frequency. The plasma frequency waves are most intense within the beam column[22] ($\gtrsim$10 V/m), falling off sharply from the beam center to the beam edge ($\sim$40 dB/m). Under these conditions, the beam electrons are redistributed in energy,[20,21] with the original peak at the accelerating potential (typically 800 V to 2 keV) broadened 10-15% FWHM (full width at half maximum), with an enhanced low-energy tail in the $E<100$ eV domain.

Following the characterization of the BPD by wave emissions, beam energy redistribution, and the various parametric dependencies, space-simulation efforts[17] then focused on determining a plasma density dependent criterion for BPD ignition. Early thoughts[17,18] suggested that the BPD was ignited when the local electron plasma frequency ω_p^e was greater than or equal to the local electron cyclotron frequency ω_c^e (i.e., $\omega_p^e\geq\omega_c^e$). This condition was found to be consistent with the most recent results,[23,24] which established

$$\overline{\omega_p^e}=5.4\omega_p^e \tag{2}$$

as the ignition criterion appropriate to the laboratory efforts at the Johnson Space Center. The density-dependent criterion also agreed with theoretical calculations that considered the BPD to be produced by large-amplitude electron plasma waves resulting from the beam-plasma interaction.

While many of the laboratory results were finding acceptable theoretical descriptions,[23,25] additional work was required to more completely define the basic plasma processes and plasma electron distributions. Critical issues included direct measurements of enhanced density levels and, more importantly, a definitive experimental determination of suprathermal electron populations at BPD threshold. Until recently the latter issue had been mostly a matter of theoretical speculation. With this in mind and with interest in exploring spectral energy transfer processes and the conversion of one type of fluctuation into another, we have conducted a number of follow-on experiments. These experiments dealt primarily with the plasma electron population, its density and energy distributions, and levels of turbulence with respect to the various BPD states (pre-, threshold-, and solid-BPD). The experimental configuration, results, and extrapolations to space-borne applications are treated in subsequent sections.

Experiment Configuration and Diagnostic Technique

The experiment was conducted in the large vacuum chamber facility at the NASA Johnson Space Center in Houston, Texas, with a configuration (Fig. 1) similar to that employed in the earlier space simulations.[17,26-28] The chamber, with base pressures $\sim10^{-6}$ Torr, was equipped with large current-carrying coils to generate magnetic fields up to 2.1 G. A steerable Pierce-type electron gun with a perveance of $\sim1.4\times10^{-6}\,AV_b^{-3/2}$ was mounted near the chamber floor on a movable cart that allowed the beam to be injected upward and parallel to the magnetic field $\bar{B}$, and to be terminated on a gridded 3×3 m collector suspended 20 m above the gun aperture.

The chamber was also equipped with a position-controlled cylindrical pulsed plasma probe[29] system (acronym P^3) that could be continuously varied in its radial position relative to the beam center. All radial traversals were along the local magnetic meridian at a height of 8 m above the gun aperture. Care was taken to guarantee that radial profile information was not distorted by magnetic-aspect sensitivities.[30]

The P^3 technique provided measurements of relative electron density on a 1-ms time scale while simultaneously generating a "conventional" Langmuir probe characteristic for determination of absolute N_e, T_e, and plasma potential V_∞. In the P^3 procedure a chain of voltage pulses are applied to the probe. The pulse amplitudes follow a sawtooth envelope and generate the data pairs (I, V) for the conventional Langmuir probe I-V characteristics. During the interpulse period the probe is held at a fixed-baseline level V_B, in the electron-saturation portion of the characteristic. The running measurements of I_B, during the baseline period V_B, provide a measure of relative N_e variations (assuming $I_B\equiv I_e^{\rm sat}\propto N_e$) and the fundamental data set for further analysis of density fluctuation power spectra. The procedure also mitigates hysteresis effects known to degrade conventional Langmuir probe procedures. (References 24 and 29 and associated bibliographies are recommended for more detailed information on the P^3 technique.) The probe was fabricated from 0.8-mm-diam tungsten wire, 20 cm in length. It was separated from an extension arm by a 2.5-cm-long coaxial guard electrode that was driven at the same potentials as the probe. The plasma currents collected by the probe were measured by an electrometer system that provided linear bipolar outputs over a current range covering five orders of magnitude.

Experimental Results

Bulk Plasma Features

To establish a framework for the plasma properties to be discussed here and in subsequent sections it is useful to adopt the three-stage description of BPD buildup proposed in the work of Getty and Smullin.[18]

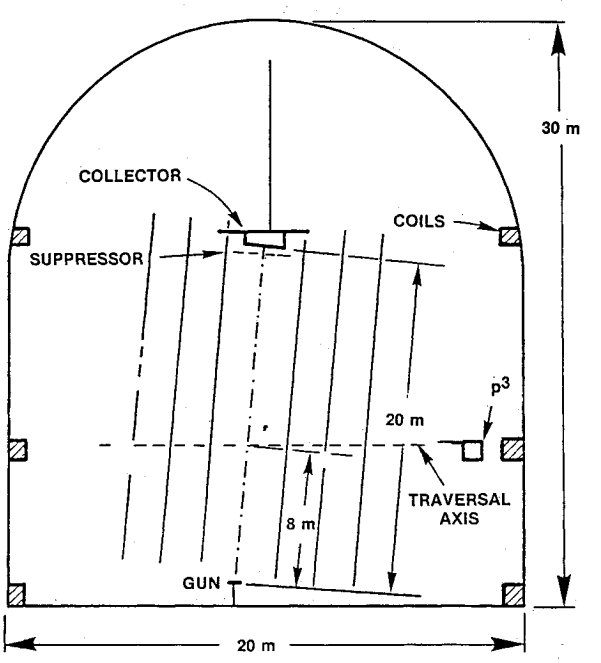

Fig. 1 Experimental configuration in the large chamber at the Johnson Space Center.

Stage 1 (Pre-BPD)

The beam behaves in the classical sense of single-particle interactions, creating ion-electron pairs upon collision with ambient neutrals. The beam-created plasma is low in density and increases linearly with beam current.

Stage 2 (Approaching Threshold)

Collective effects begin to take place with the beam-plasma system generating oscillations that first appear near the electron cyclotron frequency. These oscillations (may) produce plasma electrons in excess of that produced directly by the beam.

Stage 3 (BPD)

More intense oscillations are generated at and above the electron plasma frequency. This is believed to be the dominant mode of interaction, resulting in substantial increases in plasma production.

While this staging process was developed to describe the temporal buildup for a pulsed beam operation with $I > I_c$, it has merit for the description of dc discharges and the development toward BPD at various beam current levels. In Fig. 2 are plotted maximum values of plasma density measured along radial plasma profiles for fixed beam energy (1.3 keV) and selected levels of beam current. The data are seen to support a threshold concept in which the rate of plasma production is enhanced at some critical current level (12 mA in Fig. 2). While the enhanced ion-pair production rate may be characterized by an avalanche breakdown, as suggested in some of the earlier space-simulation efforts, there are cases in which the transition has been found to be more gradual. Experience accumulated to date indicates that at threshold $N_e(I \geq I_c)/N_e(I \leq I_c)$ never exceeds 20, with factors in the range of 2-5 being more typical.

Radial profiles of plasma density for pre-, threshold-, and solid-BPD conditions are presented in Figs. 3 and 4 for $V_b = 1.9$ and 1.3 keV, respectively. The abscissa is time relative to the start of each radial traversal, and the ordinate is the logarithm of relative electron density as determined by baseline electron saturation currents collected by the cylindrical pulsed plasma probe. At the start of each traversal the probe was at its outermost position relative to the center of the chamber and the beam axis. As time increased, the probe was moved into and through the beam at a rate ~7.5 cm/s; after penetration through the beam center the traversal system was reversed, allowing a second measurement of the density profile as the probe moved back to its original outermost position. With this procedure the probe's maximum penetration into and through the beam is identified by the symmetry point (see, e.g., top panel of Fig. 3) in the "double" profile.

The top panel in Fig. 3 is typical of a pre-BPD profile in that the beam center is well defined and of relatively narrow cross section. At BPD threshold the plasma expands in cross section generally eliminating the narrow beam profile characteristic of the pre-BPD state. As the beam current is increased above the threshold level, the plasma density increases and the radial profiles take on various configurations. For example, in the bottom panel of Fig. 3, the center is depleted with an increased density level at its edges. This configuration has been observed in a number of cases and is thought to be the result of electron heating in the beam core with generally higher diffusion rates and associated losses. The fact that a similar depletion is not observed in the bottom panel of Fig. 4 indicates that our understanding is less than complete. In fact, the results in Fig. 4 have been selected to present information at a higher magnetic field (1.5 G in Fig. 4 and 0.9 G in Fig. 3), and, to illustrate that, the description of

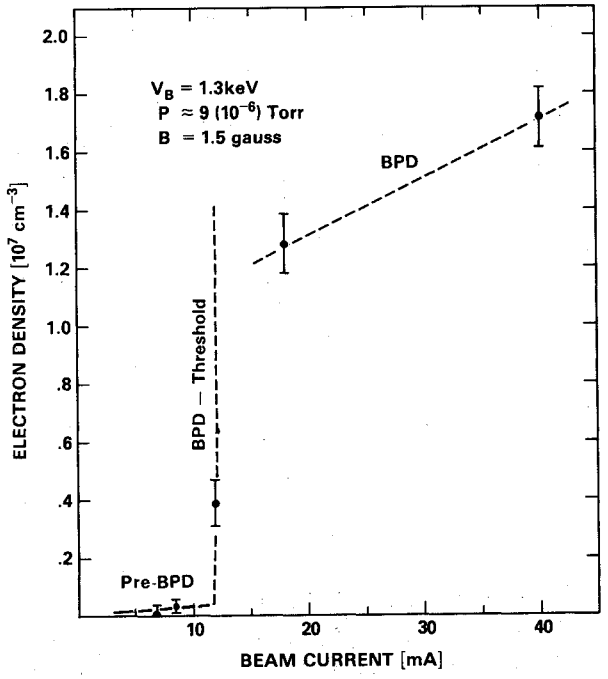

Fig. 2 Maximum values of electron density observed in radial plasma profiles at levels of beam current spanning the pre-, threshold-, and solid-BPD regimes.

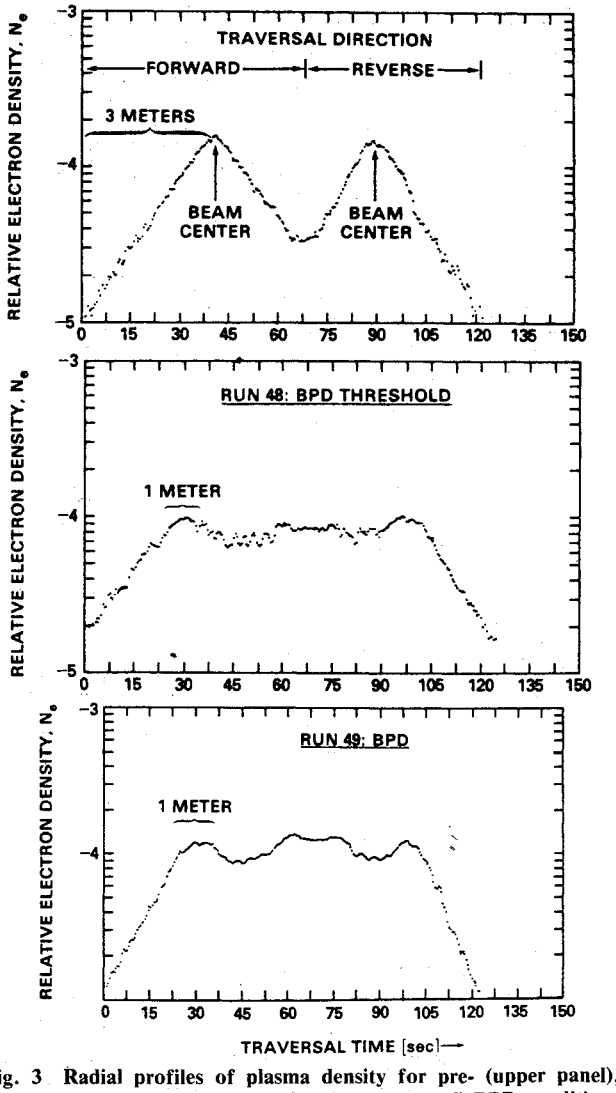

Fig. 3 Radial profiles of plasma density for pre- (upper panel), threshold- (middle panel), and solid- (bottom panel) BPD conditions at $V_b = 1.9$ keV and $B = 0.9$ G.

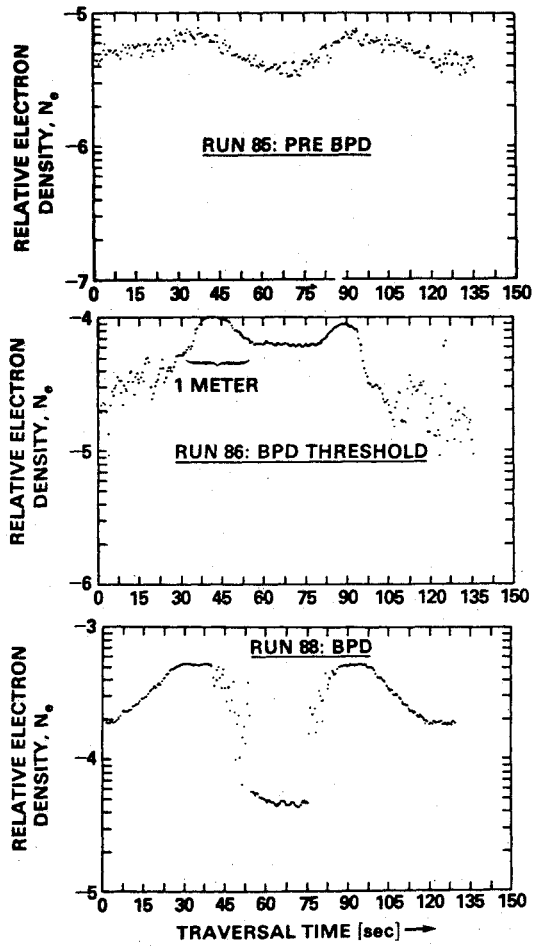

Fig. 4 Radial profiles of plasma density for pre- (upper panel), threshold- (middle panel), and solid- (bottom panel) BPD conditions at $V_b = 1.3$ keV and $B = 1.5$ G.

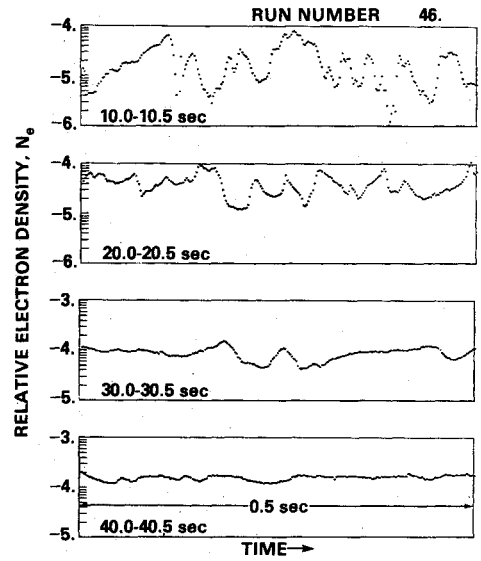

Fig. 5 A series of 0.5-s data segments showing density fluctuations at four positions within the radial profile shown in the upper plane of Fig. 3. The times displayed within each panel can be directly cross referenced with the traversal time (and relative position with respect to the beam center) in the top profile in Fig. 3.

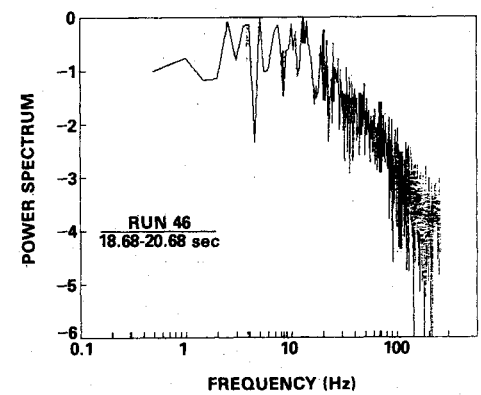

Fig. 6 FFT analysis of a 2-s segment in the profile shown in the upper panel of Fig. 3. The Fourier analyzed data sample includes the 20.0-20.5-s segment displayed in Fig. 5.

beam plasma profiles offered in connection with Fig. 3 should be considered nominally in agreement with overall observations but not universally applicable to the various levels of the BPD. (For purposes of perspective in the development of BPD, it is noted that the profiles in the upper, middle, and bottom panels of Fig. 4 correspond to the 8-, 12-, and 38-mA cases, respectively, in Fig. 2.)

Density Fluctuations

The density profiles shown in Figs. 3 and 4 are constructed of 1-s averages along the probe traversals. The actual profiles are not as uniform as the figures would suggest, but are subject to rather large-scale radially dependent density fluctuations. As an illustration, Fig. 5 presents 0.5-s segments of density fluctuations at four positions relative to the beam center under the pre-BPD conditions corresponding to the top panel in Fig. 3. In addition to frequency components easily discernible on a 0.5-s time frame, the data in Fig. 5 show that the relative fluctuation amplitude increases with radial distance from the beam center. The frequency components have been fast-Fourier analyzed (see Fig. 6) to determine the spectral distribution. The spectrum shows a dominance at the low-frequency end (1 Hz$\lesssim f \lesssim$20 Hz), with components at higher frequencies ($f \rightarrow 250$ Hz) exhibiting an f^{-3} dependence.

The radial dependence of fluctuation amplitudes is presented from two perspectives in Figs. 7 and 8. Both figures cover the pre-BPD conditions in the top panel of Fig. 3. In Fig. 7 is plotted the maximum spectral intensity measured in a radially dependent series of fast-Fourier analyzed density fluctuations. Each data point represents a Fourier analyzed block of density irregularities at specific positions in the profile, and the variations from point-to-point reflect the nondeterministic nature of the plasma turbulence. The solid curve is a smooth fit to the results and defines more quantitatively the radially-dependent fluctuation-amplitude distribution evident in the raw data (Fig. 5). The results show that the relative spectral intensity of density fluctuations in the beam-plasma system is a factor of 10-20 times greater at a 3-m distance from the beam center than it is within the beam core itself.

A similar observation (though somewhat different on a quantitative scale) is reflected in the results of Fig. 8, where $|\delta N_e|/N_e (\propto |\delta I_B|/I_B)$ is plotted in a horizontal frame that corresponds identically with the abscissa (and the conditions) in the top panel of Fig. 3. The plotted points, which are absolute deviations from sliding linear detrends, show that the fluctuations are largest outside the beam center, with the greatest frequency of occurrence at fluctuation amplitudes $\lesssim 1.0$ (i.e., less than or equal to 100% fluctuations). On a less frequent basis, the amplitude fluctuations can extend to 2.0 (i.e., 200%). Toward the beam center the fluctuation amplitude is observed at significantly reduced levels, corresponding approximately to 0.2 (20%).

The trend in density fluctuations represented in Figs. 5, 7, and 8 can be considered typical for most beam-plasma in-

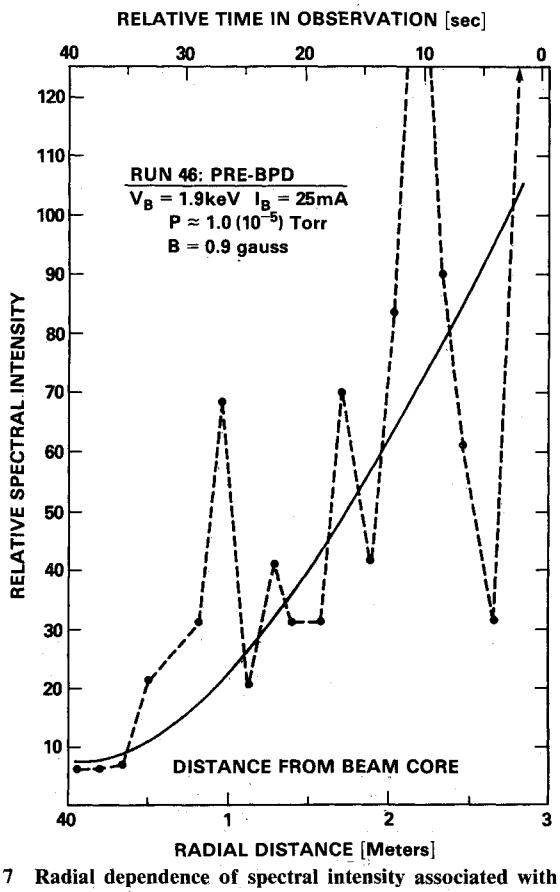

Fig. 7 Radial dependence of spectral intensity associated with the density fluctuations measured under the conditions of Fig. 3, top panel (pre-BPD condition). In each case the intensities represent peak values in the overall spectral distribution.

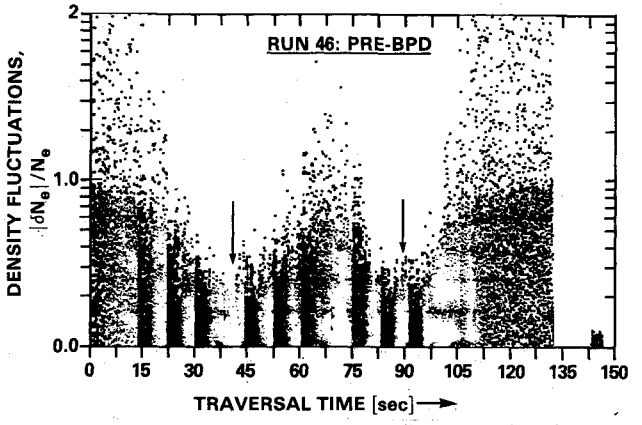

Fig. 8 Radial distribution of density fluctuations $|\delta N_e|/N_e$ occurring in the pre-BPD conditions of Fig. 3, top panel. The light and dark vertical stratifications are a result of computer-plotter anomalies.

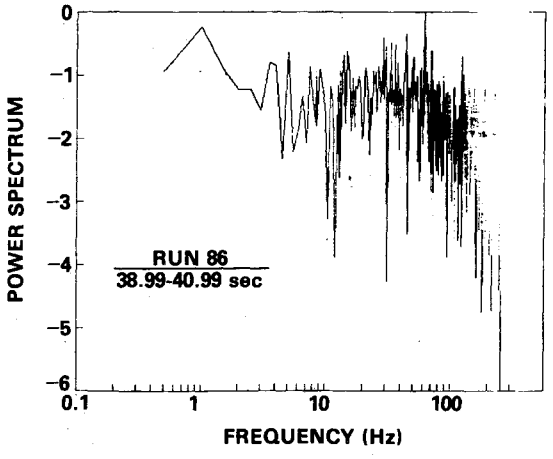

Fig. 9 FFT analysis of a 2-s segment in the threshold-BPD profile shown in the middle panel of Fig. 4.

teractions studied to date in the Johnson Space Center facility.

In an effort to identify the wave modes responsible for the observed density fluctuations, it is of benefit to return to the subject of spectral distributions. Figure 9 presents a fast-Fourier analyzed sample of density fluctuations observed under the threshold conditions in the middle panel of Fig. 4. This sample has been selected because it reflects substantial contributions from higher-frequency components ($f \rightarrow \approx 55$ Hz), and because additional attention will be given to that same threshold condition in the next section. In composite, the results in Figs. 6 and 9 are typical of the spectral observations accumulated to date: 1) Generally the density fluctuations are dominated by low-frequency components (~1-50 Hz), with relatively constant levels of intensity. 2) While observed frequencies extend to 250 Hz (higher-frequency components have as yet not been studied), the region at or near the ion cyclotron frequency (50 Hz in Fig. 9) appears to manifest the highest frequency components of substantial spectral intensity. 3) When observed, the ion cyclotron component is never a narrow peak in the spectral distribution but rather a broad feature centering at or near $\omega_c^i/2\pi$.

While the current set of observations does not provide the wavenumber measurements to complement the frequency spectrum results, the domain of contributing wave phenomena can be isolated by reference to Fig. 10. For parametric ranges encompassing the conditions in the space-simulation experiments, the figure presents the results of linear theory for the wavenumber dependence of low-frequency fluctuations extending from the lowest frequency ion acoustic waves (at 1 Hz) to whistler and Alfvén waves at 100 kHz.

Limiting the discussion to the more intense frequencies in the measurements of density fluctuations (i.e., 1 Hz$\leq f \leq$55 Hz) and to wavelengths compatible with the system size (20 m and less), it appears that there are three likely contributions: 1) the longitudinal ion cyclotron waves branching into the ion acoustic mode, 2) the lower branch of the drift wave mode, which in itself covers all frequencies in the current set of observations, and 3) a coupled drift-/ion-acoustic mode.

The existence of gradients in density and temperature (detailed below) favor the drift wave mode.

A Complete Plasma Profile

Thus far, attention has been directed to absolute densities, density fluctuation power spectra, and associated macroscopic features relevant to the various stages of beam-plasma interaction. However, a more complete analysis of the interactive beam-plasma processes requires a study of the possible effects on electron energy distribution functions. Since work on the beam electron distribution has already been reviewed, we concentrate here on the thermal electron population and the existence of suprathermal electron tails, as suggested in recent theoretical descriptions of the beam-plasma discharge.[23] A composite experimental profile of pertinent plasma parameters measured simultaneously by the P^3 diagnostic system is presented in Fig. 11 for the threshold condition corresponding to the middle panel of Fig. 4. All data for the composite profile were extracted from P^3 characteristics, with a sample in Fig. 12 showing a two-component electron population within the beam core. All related analyses assume both components to be Maxwellian

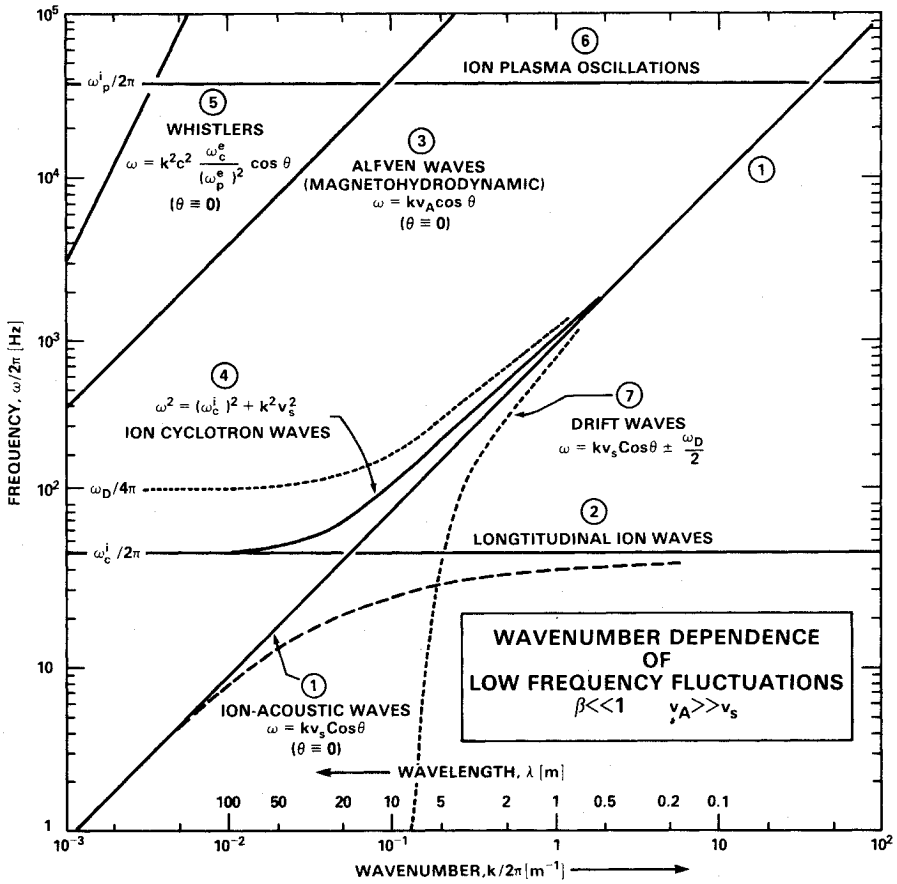

Fig. 10 Dispersion relations for low-frequency fluctuations in a magnetoplasma. The following parametric values have been assumed: $N_e = N_i = 10^6$ cm^{-3}, $T_e = 3000$ K, $M_i = 30$ amu, and $B = 1$ G.

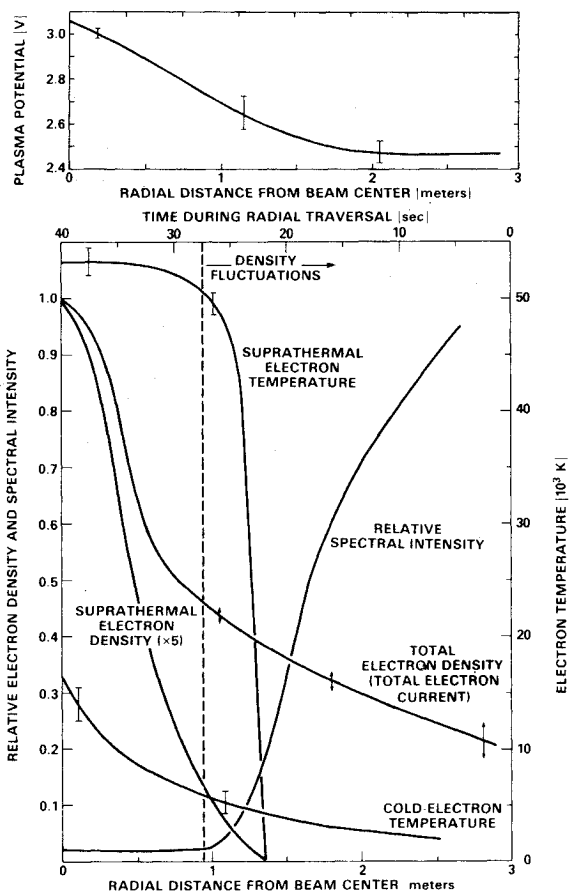

Fig. 11 Composite profile of measured plasma parameters under the BPD-threshold conditions in the middle panel of Fig. 4. Actual data points are not included in the figure, but selected error bars have been utilized to represent the data spread about the smoothed fit. Note that all curves are plotted on a linear scale.

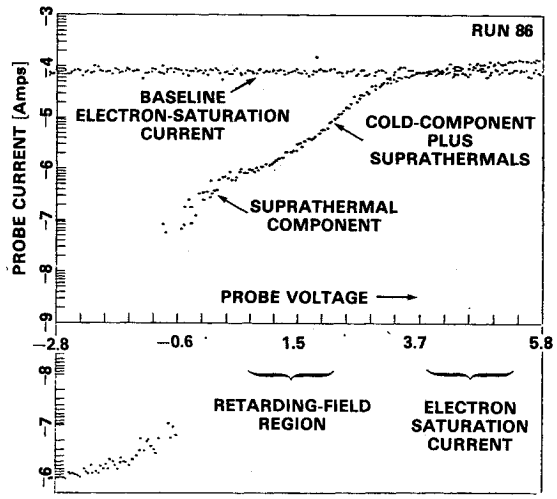

Fig. 12 Pulsed plasma probe characteristic showing evidence of a suprathermal electron component.

and characterized by an electron temperature. Accordingly, the retarding field and plasma potential domains were analyzed with conventional procedures normally employed in such environments.

The results show the suprathermal electron population confined to a region within 1 m of the beam center, with the total population falling to its e-fold level in 60-70 cm. The steep radial dependence of the suprathermal component is similarly reflected in the relative profile of the total electron density. At its peak density level, 8×10^5 cm^{-3}, the suprathermal component is 20% of the total population.

The temperature of the suprathermal component is seen to rise very sharply at the first appearance of the hot electrons near 1.3 m and then levels off to a near constant 5.3×10^4 K level near the center. The cold electron component is

1.5×10^4 K at its peak, falling off exponetially with radius, in agreement with previously reported BPD observations.[26]

The figure also reveals an interesting feature relative to the coincident measurements of density fluctuations. The dashed line marking the spatial onset of density fluctuations (an exact 1:1 temporal correspondence can be located in the time-dependent radial traversal in the central panel of Fig. 4) is colocated with an exponential-like increase in the relative spectral intensity and, more significantly, with the steep temperature gradient in the suprathermal electron population. The observation suggests that the turbulence is initiated at this suprathermal temperature boundary and expands radially with increasing amplitude as the waves penetrate lower plasma density domains.

One final observation is included in the upper panel of Fig. 12, where measurements of plasma potential are plotted in the same radial format as density, temperature, and spectral intensity. It is seen that the plasma potential is a well-behaved function, increasing in magnitude (relative to the chamber wall) with decreasing radius. The overall potential drop is only 0.6 V, corresponding to $\sim 1\ kT_e$ for an average cold electron temperature of 8×10^3 K.

Comments and Conclusions

Although the beam-plasma discharge has had a relatively long history of laboratory investigations, recent space-related efforts have brought about a renewed interest, with concerted theoretical and experimental work focusing on the problem. Accumulated information has helped expand many of the original concepts, and several new quantitative aspects of the problem have evolved. The progress has resulted in part from the improved understanding of the energization processes of the ambient plasma in its interactions with the energetic electron beam. Another major contribution has come from the team effort in attacking the problem with a perspective that concentrates on a more comprehensive description (both theoretical and experimental) of the interaction process, including diagnostics of the waves, fields, particle densities, and energy distribution functions. While the efforts reported in the present investigation have dealt only with the plasma-electron properties, an understanding of the observations was made possible only within the context of all accumulated information. The new results are:

Quantification of density enhancement in the transition from single-particle to the collective BPD process. While the BPD-enhanced ion-pair production rate may be characterized by an avalanche breakdown, as suggested in the results of Fig. 2, there are cases in which the transition is more gradual. Experience accumulated to date indicates that at BPD threshold the enhancement never exceeds 20, with factors in the range 2-5 appearing more typical.

Radial profile characterization as a function of pre-BPD, threshold, and BPD conditions. The pre-BPD plasma electron profile is well defined and of relatively narrow cross section. The beam-width itself is on the order of tens of centimeters, with the plasma density falling exponentially to the chamber walls. At BPD threshold the plasma column expands in cross section (1-2 m), generally eliminating the narrow beam profile characteristic of the pre-BPD state. As the beam current is increased above BPD threshold, the plasma density increases and the density profiles take on various configurations, with evidence for electron heating in the beam core and generally higher diffusion rates. (See Figs. 3 and 4.)

Amplitude and spectral classification of density fluctuations. Density fluctuations are dominated by low-frequency components ($\sim$1-50 Hz), with amplitudes increasing with distance from the beam center. Fluctuation levels can reach 100%. Candidate wave modes include 1) longitudinal ion cyclotron waves branching into ion acoustic modes, 2) the lower branch of the drift wave mode, and 3) a coupled drift-/ion-acoustic mode. The presence of steep gradients in density and temperature favor the latter mode as dominant.

Identification and mapping of the suprathermal electron component at and above BPD threshold. Copious amounts of suprathermal electrons were found to coincide with the onset of BPD. These electrons ($N_e = 8 \times 10^5$ cm^{-3} at 5 eV) are part of a broad distribution that extends up through the 50-100 eV range.[31] They result from strong wave-particle interactions and trigger the enhanced ionization process characteristic of the BPD. Their observation represents an important step in experimental studies of beam-plasma interactions and significantly improve the developing model of the BPD.

Acknowledgments

It is with great pleasure that the contributions and discussions of the entire TEBPP Science Team be acknowledged. Valuable input has been provided by W. Bernstein, K. Papadopoulos, H. Anderson, H. Leinbach, P. Kellogg, J. C. Holmes, D. N. Walker, T. Hallinan, J. R. Jost, L. Linson, R. Holtzworth, and P. Rodriguez. In addition, the diligent, competent, and dedicated data processing of C. S. Lin is most gratefully acknowledged. Development of the P^3 technique and support for data reduction and analysis was provided by the Office of Naval Research under Work Unit 41-0949, Ionospheric and Magnetospheric Interactions, Task Area RR 043-02-44. Support for the experiment was provided under NASA/NOAA Contract NA79RAA04487.

References

[1] Langmuir, I., "Scattering of Electrons in Ionized Gases," *Physical Review*, Vol. 26, Nov. 1925, pp. 585-613.

[2] Penning, F. M., "Uber die Ionisation durch Elekronen in einem homogenen elektrischen Felde," *Zeitschrift fur Physik*, Vol. 40, Oct. 1926, pp. 4-11.

[3] Langmuir, I. and Tonks, L., "Oscillations in Ionized Gases," *Physical Review*, Vol. 33, Feb. 1929, pp. 195-210.

[4] Bohm, D., Burhop, E., Massey, H. S. W., and Williams, R., "A Study of the Arc Plasma," *The Characteristics of Electrical Discharges in Magnetic Fields*, edited by A. Guthrie and R. K. Wakerling, McGraw-Hill Book Co., New York, 1949.

[5] Hess, W. N. et al., "Artificial Aurora Experiment: Experiment and Principal Results," *Journal of Geophysical Research*, Vol. 76, Aug. 1971, pp. 6067-6081.

[6] Davis, T. N., Hallinan, T. J., Mead, G. O., Mead, J. M., Trichel, M. C., and Hess, W. N., "Artificial Aurora Experiment: Ground-Based Optical Observations," *Journal of Geophysical Research*, Vol. 76, Aug. 1971, pp. 6082-6092.

[7] Cambou, F. et al., "The Zarnitza Rocket Experiment on Electron Injection," *Space Research*, Vol. XV, edited by M. J. Rycroft, Akademie-Verlag, Berlin, 1975, p. 491.

[8] Cartwright, D. G. and Kellogg, P. J., "Observations of Radiation from an Electron Beam Artificially Injected into the Ionosphere," *Journal of Geophysical Research*, Vol. 79, April 1974, pp. 1439-1457.

[9] Cambou, F. et al., "ARAKS-Controlled or Puzzling Experiment?," *Nature*, Vol. 271, Feb. 1978, pp. 723-726.

[10] O'Neil, R. R., Bien, F., Burt, D., Sandock, J. A., and Stair, A. T. Jr., "Summarized Results of the Artificial Auroral Experiment, Precede," *Journal of Geophysical Research*, Vol. 83, July 1978, pp. 3273-3280.

[11] Galeev, A. A., Mishin, E. V., Sagdeev, E. V., Shapiro, R. Z., and Shevchenko, I. V., "Discharge in the Region Around a Rocket Following Injection of Electron Beams into the Ionosphere," *Soviet Physics Doklady*, Vol. 21, 1976, p. 641 (English translation).

[12] Hendrickson, R. A., McEntire, R. W., and Winckler, J. R., "Electron Echo Experiment: A New Magnetospheric Probe," *Nature*, Vol. 230, April 1971, pp. 564-566.

[13] Winckler, J. R., "Investigation of Electron Dynamics in the Magnetosphere with Electron Beams Injected from Sounding Rockets," *Journal of Geophysical Research*, Vol. 40, Aug. 1974, pp. 729-749.

[14] Winckler, J. R., "The Application of Artificial Electron Beams to Magnetospheric Research," *Reviews of Geophysics and Space Physics*, Vol. 18, Aug. 1980, pp. 659-682.

[15] Bernstein, W. et al., "Laboratory Observations of RF Emissions at ω_{pe} and $(N+\frac{1}{2})\omega_{ce}$ in Electron Beam-Plasma Interactions," *Journal of Geophysical Research*, Vol. 80, Nov. 1975, pp. 4375-4379.

[16] Bernstein, W. et al., "Electron Beam Experiments: The Beam Plasma Discharge at Low Pressures and Magnetic Field Strengths," *Geophysical Research Letters*, Vol. 5, Feb. 1978, pp. 127-130.

[17] Bernstein, W., Leinbach, H., Kellogg, P. J., Monson, S. J., and Hallinan, T., "Further Laboratory Measurements of the Beam-Plasma-Discharge," *Journal of Geophysical Research*, Vol. 84, Dec. 1979, pp. 7271-7278.

[18] Getty, W. D. and Smullin, L. D., "Beam Plasma Discharge: Buildup of Oscillations," *Journal of Applied Physics*, Vol. 34, Dec. 1963, pp. 3421-3429.

[19] Smullin, L. D., "A Review of the Beam-Plasma Discharge," *Relation Between Laboratory and Space Plasmas*, edited by H. Kikuchi, D. Reidel Publishing Co., Boston, 1981, p. 4566.

[20] Jost, R. J., Anderson, H. R., and McGarity, J. O., "Electron Energy Distributions Measured During Electron Beam-Plasma Interactions," *Geophysical Research Letters*, Vol. 7, July 1980, pp. 509-512.

[21] Anderson, H. R., Jost, R. J., and Gordenk, J., "Electron Energy Distribution Produced by Beam-Plasma-Discharge," *Artificial Particle Beams in Space Plasma Physics*, edited by B. Grandal, Plenum Publishing Co., New York, 1982, pp. 351-359.

[22] Jost, R. J., Anderson, H. R., and Bernstein, W., "Radial Dependence of the hf Wave Field-Strength in the BPD Column," *Artificial Particle Beams in Space Plasma Physics*, edited by B. Grandal, Plenum Publishing Co., New York, 1982, pp. 431-437.

[23] Papadopoulos, K., "Theory of Beam-Plasma Discharge," *Artificial Particle Beams in Space Plasma Physics*, edited by B. Grandal, Plenum Publishing Co., New York, 1982, pp. 505-524.

[24] Szuszczewicz, E. P., Papadopoulos, K., Bernstein, W., Lin, C. S., and Walker, D. N., "Threshold Criteria for a Space-Simulation Beam-Plasma-Discharge," *Journal of Geophysical Research*, Vol. 87, March 1982, pp. 1565-1573.

[25] Rowland, H. L., Chang, C. L., and Papadopoulos, K., "Scaling of the Beam-Plasma-Discharge," *Journal of Geophysical Research*, Vol. 86, Oct. 1981, pp. 9215-9218

[26] Szuszczewicz, E. P., Walker, D. N., and Leinbach, H., "Plasma Diffusion in a Space Simulation Beam-Plasma Discharge," *Geophysical Research Letters*, Vol. 6, March 1979, pp. 201-204.

[27] Kellogg, P. J. et al., "Laboratory Simulation of Injection of Particle Beams in the Ionosphere," *Artificial Particle Beams in Space Plasma Physics*, edited by B. Grandal, Plenum Publishing Co., New York, 1982, pp. 289-329.

[28] Szuszczewicz, E. P. and Lin, C. S., "Time-Dependent Plasma Behavior Triggered by a Pulsed Electron Gun Under Conditions of Beam-Plasma Discharge," *Artificial Particle Beams in Space Plasma Physics*, edited by B. Grandal, Plenum Publishing Co., New York, 1982, pp. 361-370.

[29] Holmes, J. C. and Szuszczewicz, E. P., "A Plasma Probe System with Automatic Sweep Adjustment," *Review of Scientific Instruments*, Vol. 52, March 1981, pp. 377-381.

[30] Szuszczewicz, E. P. and Takacs, P. Z., "Magnetosheath Effects on Cylindrical Langmuir Probes," *Physics of Fluids*, Vol. 22, Dec. 1979, pp. 2424-2429.

[31] Szuszczewicz, E. P., Anderson, H. R., Papadopoulos, K., and Walker, D. N., "Direct Measurements of Suprathermal Electron Tails in a Space-Simulation Beam-Plasma-Discharge, *EOS*, Vol. 63, May 1982, p. 408.